# Structural and magnetic properties of $Fe_xMn_{1-x}$ thin films on Cu(001) and on Co/Cu(001)

F. Offi, W. Kuch, and J. Kirschner
*Max-Planck-Institut für Mikrostrukturphysik, Weinberg 2, D-06120 Halle, Germany*
(Received 19 February 2002; revised manuscript received 18 June 2002; published 16 August 2002)

The structural and magnetic properties of $Fe_xMn_{1-x}$ alloy thin films deposited on Cu(001) and on Co/Cu(001) are investigated. A layer-by-layer growth mode of the alloy films in a large range of concentration is deduced from the presence of regular oscillations in medium-energy electron-diffraction intensity. Low-energy electron-diffraction experiments reveal that $Fe_{50}Mn_{50}$ films keep the fcc structure when growing on Cu(001) and on Co/Cu(001). Magneto-optic Kerr effect is used to study the magnetic properties of Co/FeMn bilayers. A temperature-dependent increase in the coercive field of the Co film, when the thickness of the adjacent FeMn film exceeds a certain value, is related to the antiferromagnetic state of the $Fe_xMn_{1-x}$ alloy.

DOI: 10.1103/PhysRevB.66.064419 PACS number(s): 75.50.Ee, 68.55.−a, 75.70.−i

## I. INTRODUCTION

The number of studies of the structural and magnetic properties of thin antiferromagnetic (AFM) films was remarkably increased over the past decade, after a bilayer composed by a ferromagnetic (FM) and an AFM material has been used in an exchange biased spin valve.[1] The interaction at the interface between the AFM and the FM materials induces just one stable direction for the magnetization of the system, leading to a unidirectional anisotropy, dubbed *exchange anisotropy*, discovered almost forty years ago by Meiklejohn and Bean.[2] Two of the manifestations of this exchange anisotropy are an increased coercive field and a hysteresis loop displaced from the origin along the applied field axis. The value of the displacement, that is, the distance between the origin of the axes and the center of the hysteresis loop, is usually called *exchange bias field* ($H_{eb}$). Despite the large number of both experimental[3] and theoretical[4] investigations still a general explanation for all the observations arising from the magnetic interaction at an FM-AFM interface is not available.

Indeed the phenomenon is inherently complex, since the interaction is realized at the interface, which is a location hard to explore experimentally, and since not all the parameters involved, such as structural perfection, influence of magnetic anisotropy, spin configuration, or domain formation, are easily controlled at the same time. One has also to take into account that AFM materials are involved, the magnetic properties of which are generally less known than the ones of FM materials, since most of the techniques used to characterize magnetic properties probe the spontaneous magnetization of the sample. A further complication arises from the incomplete characterization of the interface conditions in sputtered films, which are frequently used in many investigations of exchange anisotropy. From this point of view single-crystal epitaxial FM/AFM bilayers seem to be better candidates in order to understand the details of the magnetic coupling, because the interface can be described by much less parameters than in sputtered polycrystalline systems and, moreover, no grains of different crystal orientation are present, which could further complicate the study of the magnetic interaction at the interface.

For these reasons thin $Fe_xMn_{100-x}$ single crystal films are characterized in this work from a structural and magnetic point of view. In bulk material, $Fe_xMn_{100-x}$ disordered alloys are antiferromagnetic with an fcc structure in a concentration range between $x=45$ at. % and $x=75$ at. % at room temperature.[5,6] The Néel temperature ($T_N$) varies with $x$ and reaches a maximum of about 500 K at $x\approx 50$ at. %. This relatively high $T_N$ of the alloy at equiatomic composition had made $Fe_{50}Mn_{50}$ one of the most used materials in spin valve structures.[7–9] Even if in many applications $Fe_{50}Mn_{50}$ has been replaced by antiferromagnetic materials with higher corrosion resistance and higher blocking temperature, such as IrMn (Ref. 10) and MnPt,[11] still it takes the character of a model system for the investigation of the magnetic coupling at the FM/AFM interfaces.

In order to preserve the fcc $\gamma$ phase in thin $Fe_{50}Mn_{50}$ films, a Cu(001) substrate has been used in this work. The lattice parameter of $Fe_{50}Mn_{50}$, $a=3.629$ Å,[6] in fact fits quite well with the one of Cu(001), $a=3.615$ Å.[12] This lattice misfit of less than 1% should promote a pseudomorphic growth of $Fe_{50}Mn_{50}$ on Cu(001), which is indeed the case, as demonstrated in this paper by means of low- and medium-energy electron diffraction. The magnetic properties of $Fe_xMn_{100-x}$ alloy films, in particular the AFM ordering temperature, are investigated by measuring magnetization curves in $Co/Fe_xMn_{100-x}$ bilayers by the magneto-optic Kerr effect (MOKE). The thickness-dependent transition from paramagnetic to antiferromagnetic in $Fe_xMn_{100-x}$ films is in fact reflected by a change in the magnetic properties of the adjacent Co film.

The paper is organized as follows. After this introduction the experimental techniques are briefly described in Sec. II. Section III contains the results of the structural and magnetic investigation, which are discussed in Sec. IV. At the end some concluding remarks are given.

## II. EXPERIMENT

The experiments were performed in an ultra-high-vacuum chamber with a base pressure of about $1\times10^{-8}$ Pa. The chamber is equipped with facilities to study the structural and magnetic properties of thin magnetic films. The Cu substrate used for growing the films was a disk-shaped single crystal with the [100] direction normal to the surface. In

 

order to obtain a clean and smooth surface the crystal was treated in the vacuum chamber by 1-keV $Ar^+$-ion bombardment and subsequent heating up to about 800 K in 3 min, keeping then this temperature for two more minutes. The temperature was controlled by an *N*-type thermocouple attached to the sample holder. The presence of contaminants on the substrate surface was checked to be below the detection limit of the Auger electron spectroscopy (AES) system ($\approx 2\%$ of a ML).

The ordered surface structure has been checked by low-energy electron diffraction (LEED), where a beam of electrons with primary energy up to $\approx 500$ eV is incident perpendicularly on the surface, and the elastically backscattered electrons produce a diffraction pattern on a fluorescent screen. Besides the two-dimensional translational symmetry at the surface, from LEED one can gain information also about the average vertical interlayer distance. Within the kinematic theory, based on the approximation that only single scattering processes occur, the vertical interlayer distance $d$ can be expressed as[13]

$$d = \frac{n\pi\hbar}{\sin\theta\sqrt{2m_e[E_p(n) - V_0]}}, \tag{1}$$

where the integer $n$ is the order of the corresponding interference peak, $E_p(n)$ the primary energy of the electrons of that peak, $V_0$ the additional energy shift due to the average inner potential in the crystal, $m_e$ the electron mass, and $\theta$ the incident angle with respect to the sample surface.

The films were grown on the clean substrate at room temperature (315 K) by electron beam-assisted thermal evaporation. Fe and Co were cut from high-purity wires (99.99% purity) of 2-mm diameter and fixed by spot-welding to a support rod inside the water-cooled evaporation source. To evaporate Mn two ways were used: either a small irregular Mn piece (99.98% purity), of dimension around 10 mm, was held by a Ta wire, or a rod (99.5% purity) of 5-mm diameter was fixed to the evaporator by a thin Ta foil wrapped around it. The second solution offered better results in terms of stability of the evaporation rate. FeMn alloys were obtained by simultaneous evaporation of Fe and Mn from two different sources. During deposition the pressure in the chamber could be kept below $5\times10^{-8}$ Pa. The rate of deposition of the growing films, typically of 0.5–1 ML per min, was checked by counting the oscillations in the specular medium-energy electron-diffraction (MEED) intensity recorded during evaporation. The geometry used to perform MEED exploits the fact that in the chamber setup the AES system is mounted face to face with the LEED system. This allows diffraction experiments in a grazing incidence geometry with primary electron kinetic energy of 2 keV, using the electron gun of the AES system and the fluorescent screen of the LEED system.

Magnetization curves have been recorded *in situ* by MOKE experiments. The MOKE setup, as described in a previous publication,[14] allows measurement of both the longitudinal and the polar Kerr signal, with a maximum available external field of about 200 Oe.

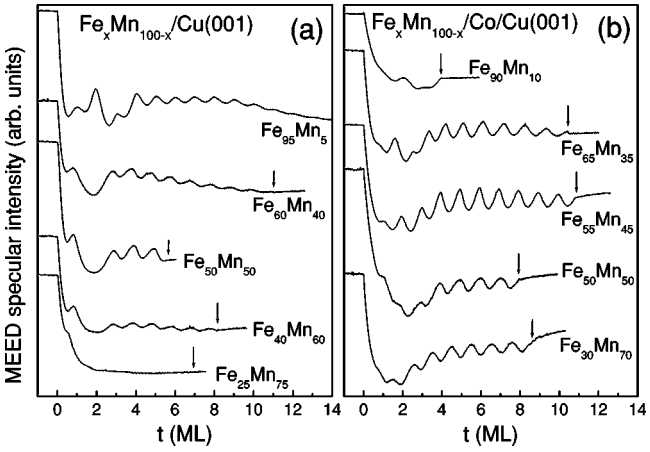


FIG. 1. MEED specular beam intensity recorded during growth at 315 K of $Fe_xMn_{100-x}$ alloy films on Cu(001) (a) and on 6-ML Co/Cu(001) (b) as a function of the FeMn thickness ($t$) in ML's. The arrows at some curves indicate the closing of the shutter in front of the evaporation sources. Each curve is labeled with the corresponding alloy film composition.

## III. RESULTS

### A. Structural properties

In order to characterize the growth properties, the specular MEED intensity has been recorded during the deposition of the films. When Fe was evaporated on top of Cu(001) an oscillatory behavior of the MEED intensity has been observed, very similar to what has already been reported.[15] MEED oscillations have also been recorded during the growth of Fe on Co/Cu(001). From the period of the MEED oscillations one can determine the evaporation rate of Fe ($r_{\mathrm{Fe}}$) in atomic monolayer (ML) units. The specular MEED intensity recorded during the growth of Mn on Cu(001) and on Co/Cu(001), however, does not display an oscillatory behavior. After the opening of the shutter in front of the evaporation source the specular MEED intensity drops down due to the initial increase of density of surface steps. Apart from a small shoulder at a thickness slightly lower than 1-ML Mn, the intensity monotonically decreases up to a thickness of $\approx 3$ ML, staying later almost constant. During the simultaneous evaporation of Fe and Mn on Cu(001) and on Co/Cu(001), oscillations in the MEED intensity are again observable. From the period of the oscillations it is possible to determine the evaporation rate ($r_{\mathrm{FeMn}}$) of the $Fe_xMn_{100-x}$ alloy films. If Fe is evaporated at the same rate for deposition of the Fe film and of the $Fe_xMn_{100-x}$ film, one can compare $r_{\mathrm{Fe}}$ and $r_{\mathrm{FeMn}}$ as determined by MEED. In this way one has the possibility to calculate the composition of the $Fe_xMn_{100-x}$ film, since $x$ is obtained by the ratio of $r_{\mathrm{Fe}}$ and $r_{\mathrm{FeMn}}$. A complementary method to cross-check thickness and composition of the $Fe_xMn_{100-x}$ film on Cu is given by AES, by using calibration curves derived from pure Fe and Mn on Cu(001).

Figure 1 shows the specular MEED intensity recorded during the growth of $Fe_xMn_{100-x}$ films on Cu(001) [Fig. 1(a)] and on 6-ML Co/Cu(001) [Fig. 1(b)] for a wide range of concentration between $x=25$ at.% to $x=95$ at.%. In

the figure the MEED intensity is displayed as a function of the FeMn thickness ($t$) in ML's. Each curve corresponds to a different film with a different concentration as indicated. The arrows present in some curves indicate the closing of the shutter in front of the evaporators. Apart from the $Fe_{25}Mn_{75}$ film on Cu(001), in all other cases the intensity presents an oscillatory behavior related to the periodic variation of the average number of surface defects.[16,17] This in turn is due to the layer-by-layer growth mode of the $Fe_xMn_{100-x}$ alloy films on Cu(001) and on Co/Cu(001), at least for the concentration range in which the oscillations are present. As pointed out previously, the period of the oscillations gives a precise way to determine the film thickness in ML units.

The presence of MEED oscillations indicates, in particular, a pseudomorphic layer-by-layer growth mode of $Fe_{50}Mn_{50}$ films deposited on Cu(001) and on a thin Co layer on Cu(001). On the other hand from the presence of MEED oscillations during the growth of Co on Cu(001) it has been deduced that a thin Co film also grows in a layer-by-layer mode on Cu(001).[18] More generally the same conclusion can be drawn for both the bilayers $Fe_{50}Mn_{50}$/Co and Co/$Fe_{50}Mn_{50}$ growing on Cu(001) as it is demonstrated in Fig. 2. In Fig. 2(a) the MEED intensity as a function of time is shown for the growth at 315 K of 6-ML Co on top on Cu(001), and the subsequent evaporation of 8-ML $Fe_{50}Mn_{50}$ on top of it. The order of evaporation is reversed in Fig. 2(b) where the MEED intensity as a function of time is displayed for the growth of a 13-ML Co/8-ML $Fe_{50}Mn_{50}$ bilayer on Cu (001). In both cases the stop of the double evaporation is indicated by the ''shutter closed'' arrow. Distinct oscillations are present for all the four layers evaporated.

To obtain information about the crystallographic structure, LEED experiments have been performed. It is particularly important, as will be pointed out in the next section, to check if $Fe_{50}Mn_{50}$ keeps the fcc structure also in the thin-film regime. Selected LEED patterns are presented in Figs. 3 and 4. Figure 3 shows the LEED pattern of the clean Cu substrate at 125-eV electron energy [Fig. 3(a)] and of a 26-ML $Fe_{50}Mn_{50}$ film on Cu(001) at 115 eV [Fig. 3(b)]. The LEED patterns appear to be quite similar for both cases. This indicates that the $Fe_{50}Mn_{50}$ film forms a $p(1\times1)$ overlayer with the substrate lattice, at least up to the maximum investigated thickness of 26 ML. A similar behavior is expected also for $Fe_{50}Mn_{50}$ films growing on a Co/Cu(001) substrate, considering that Co acquires the same in-plane lattice parameter as Cu when deposited on top of it.[18] In Fig. 4 the result of the investigation on the first stages of growth of an $Fe_{50}Mn_{50}$ film on 6-ML Co/Cu(001) is reported. LEED patterns are shown for the Cu(001) substrate [Fig. 4(a)], 6-ML Co/Cu(001) [Fig. 4(b)], 0.5-ML $Fe_{50}Mn_{50}$/6-ML Co/Cu(001) [Fig. 4(c)], and 2-ML $Fe_{50}Mn_{50}$/6-ML Co/Cu(001) [Fig. 4(d)]. Again in all images a very similar diffraction pattern can be seen. As stated above, a thin Co film forms a $p(1\times1)$ overlayer on Cu(001), as one can see by comparing Figs. 4(a) and 4(b). The same holds also for the growth of the first ML's of $Fe_{50}Mn_{50}$ on Co/Cu(001). Moreover, one realizes that in the diffraction patterns of the initial stages of growth of $Fe_{50}Mn_{50}$ on Co/Cu(001), see Figs. 4(c) and 4(d), no superstructures are formed, as could be in the case of alloying with the underlying layer. The absence of a superstructure, however, does not prove that no alloying exists at the interface.

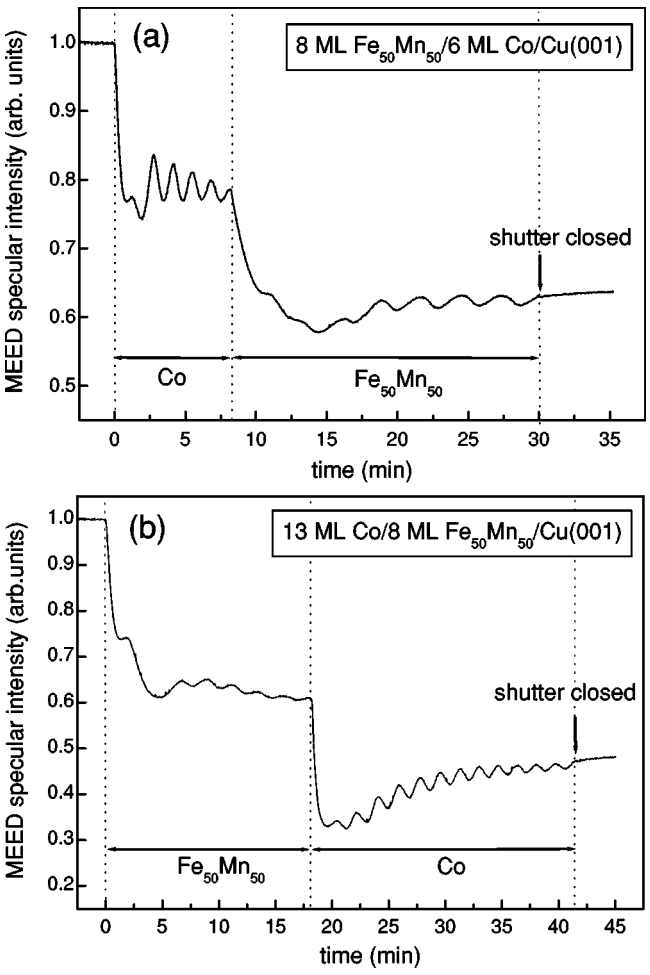


FIG. 2. MEED specular beam intensity as a function of time during the deposition of 8 ML $Fe_{50}Mn_{50}$/6-ML Co on Cu(001) (a) and 13-ML Co/8-ML $Fe_{50}Mn_{50}$ on Cu(001) (b). The starting of the evaporation of the bilayer corresponds to the time 0. The evaporation ends at the time indicated as ''shutter closed.'' The presence of oscillations in the intensity is characteristic for a pseudomorphic layer-by-layer growth mode.

Besides the lateral arrangement of the atoms, from LEED one can also extract information about the vertical average

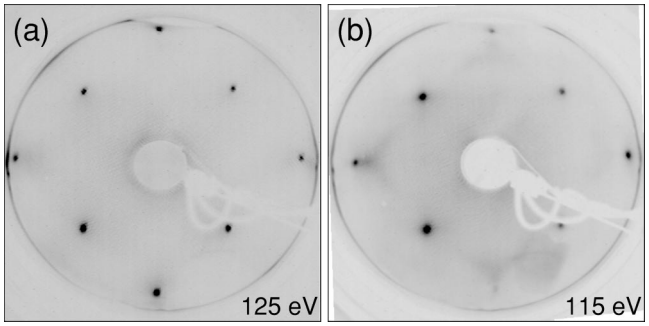


FIG. 3. LEED patterns from the clean Cu(001) substrate (a), and a 26-ML-thick $Fe_{50}Mn_{50}$ film on Cu(001) (b). The primary energy of the electrons is indicated.

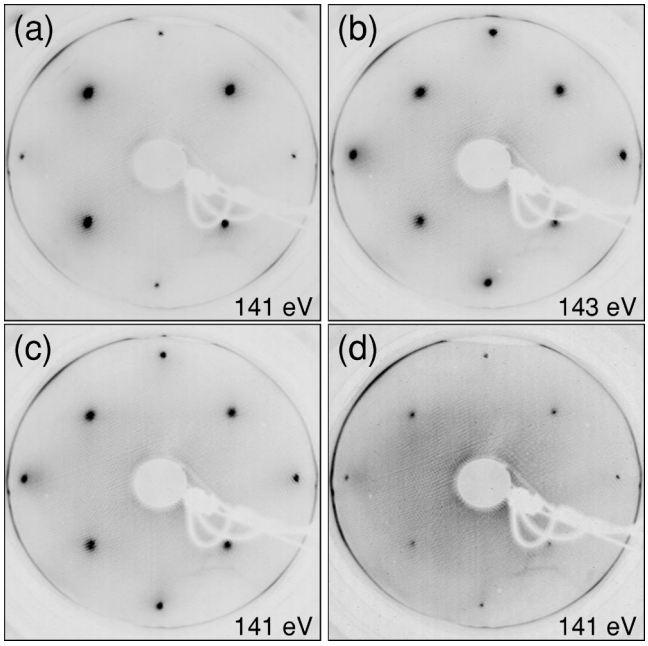


FIG. 4. LEED patterns from the clean Cu(001) substrate (a), 6-ML Co/Cu(001) (b), 0.5-ML $Fe_{50}Mn_{50}$/6-ML Co/Cu(001) (c), and 2-ML $Fe_{50}Mn_{50}$/6-ML Co/Cu(001) (d). The primary energy of the electrons is indicated.

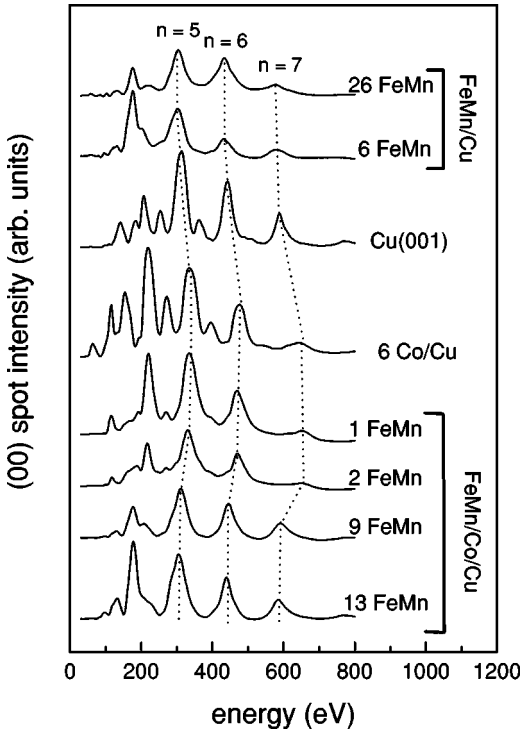


FIG. 5. Intensity versus energy dependence of the LEED (00) beam for $Fe_{50}Mn_{50}$ films grown on Cu(001) (top part of the figure) and on 6-ML Co/Cu(001) (bottom part of the figure). For comparison also the $I(E)$ curves for the Cu substrate and the 6-ML Co/Cu(001) are shown. The label at each curve indicates the layer thicknesses. The integer $n$ labels the order of the single scattering Bragg maximum. The $I(E)$ curves have been obtained at a polar angle of 5° from the surface normal, and at an azimuth angle corresponding to the ⟨100⟩ crystallographic direction of the Cu(001) substrate.

interlayer distance. This information is obtained by recording the intensity $I$ of the (00) diffracted spot as a function of the primary electron energy $E$. Selected $I(E)$ curves are reported in Fig. 5 for several $Fe_{50}Mn_{50}$ films grown on Cu(001) (top part of the figure) and on 6-ML Co/Cu(001) (bottom part of the figure). The labels at each curve indicate the layer thicknesses. The composition of the $Fe_{50}Mn_{50}$ films is omitted in the labels for brevity. For comparison also the $I(E)$ curves for the Cu substrate and the 6-ML Co/Cu(001) are shown. The integer $n$ labels the order of the single-scattering Bragg maximum. The intensity of the maxima is somehow lower for the films than for the Cu(001) substrate, but the peaks are visible up to the maximum thicknesses reported. Within the kinematic theory, using Eq. (1), from the $I(E)$ curves one can calculate the average value of the interlayer distance near the surface. The result is shown in Fig. 6 as a function of the $Fe_{50}Mn_{50}$ film thickness ($t_{FeMn}$), expressed in ML's. In the figure the horizontal dashed line at 1.808 Å indicates the vertical interlayer distance in bulk Cu(001),[12] the dash-dotted line at 1.815 Å the vertical interlayer distance in bulk $Fe_{50}Mn_{50}$,[6] and the dotted line at 1.74 Å the vertical interlayer distance for 6-ML Co on Cu(001),[18] as taken from literature. When grown on Cu(001), the Co lattice is in fact slightly tetragonally compressed because of the lattice mismatch between the fcc Co and Cu unit cells. The open square and the solid circle indicate the experimental values for the Cu(001) substrate and the 6-ML Co/Cu(001) film respectively, as indicated by the labels. The solid squares are the vertical interlayer distances for $Fe_{50}Mn_{50}$ films grown on Cu(001). One can see that within the experimental error all the points agree with the value of Cu(001), which is actually very close to the value of bulk $Fe_{50}Mn_{50}$. A small vertical

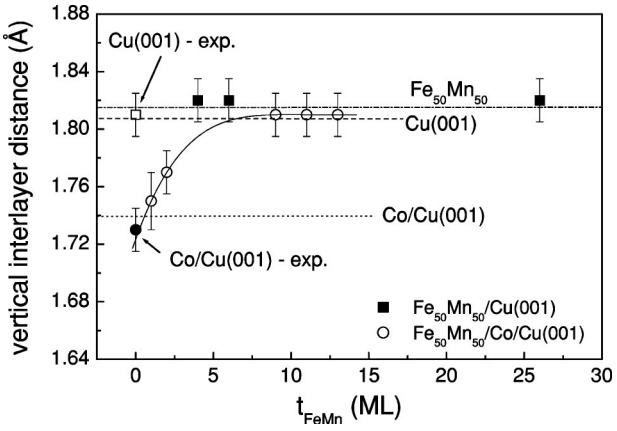


FIG. 6. Vertical interlayer distance as a function of $Fe_{50}Mn_{50}$ thickness ($t_{FeMn}$), for films grown on Cu(001) (filled squares), and on 6-ML Co/Cu(001) (open circles). The open square and the filled circle indicate the experimental values of vertical interlayer distance for the Cu(001) substrate and the 6-ML Co/Cu(001) film, respectively. The dashed, dash-dotted, and the dotted lines are the values of interlayer distances for bulk Cu(001), bulk $Fe_{50}Mn_{50}$, and 6 ML Co/Cu(001), respectively, as taken from literature.

expansion of the $Fe_{50}Mn_{50}$ lattice, for $Fe_{50}Mn_{50}$ films growing on Cu(001), as a consequence of the lateral misfit with the Cu(001) substrate, can not be completely ruled out. A hint of this expansion can be seen from the $I(E)$ curves of FeMn films on Cu(001) of Fig. 5, where the Bragg maxima are slightly shifted towards lower energy compared to the $I(E)$ curve of the pure Cu substrate. The open circles in Fig. 6 are the values of the interlayer distance for $Fe_{50}Mn_{50}$ films grown on 6 ML Co/Cu(001). The solid line connecting the open circles is a guide to the eye. The two points for low $Fe_{50}Mn_{50}$ thickness, at 1 and 2 ML, are still quite close to the value of the Co film. This is most likely due to the fact that what is measured here is an *average* value, and for low $Fe_{50}Mn_{50}$ thickness the contribution of the underlying Co film is still quite large. For higher $Fe_{50}Mn_{50}$ thickness the vertical interlayer distance is again very close to the values of bulk Cu(001) and $Fe_{50}Mn_{50}$. The above results are therefore pointing to the conclusion of an epitaxial growth of the $Co/Fe_{50}Mn_{50}$ bilayers on Cu(001). Moreover, the fcc crystalline structure of the substrate is preserved also in the grown bilayers.

### B. Magnetic properties

As mentioned in the introduction, in the bulk, the $Fe_{50}Mn_{50}$ alloy is an antiferromagnet with a $T_N \approx 500$ K.[6] Thin $Fe_{50}Mn_{50}$ films deposited on Cu(001), measured in this work, do not show any ferromagnetic signal at room temperature both in the longitudinal and in the polar MOKE geometry, as measured up to an $Fe_{50}Mn_{50}$ thickness $t_{\mathrm{FeMn}} = 20$ ML. This is in agreement with the non-FM state of the alloy also in the thin-film regime. To probe the AFM ordering, the change in the magnetic properties of an adjacent Co film has been measured. In a typical experiment, hysteresis loops in the longitudinal MOKE geometry were recorded at room temperature upon increasing $t_{\mathrm{FeMn}}$ by subsequent evaporation steps on top of 6-ML Co/Cu(001). The external field was applied along the [110] azimuth direction of the substrate, which is the easy axis of magnetization of a thin Co film grown on Cu(001).[19,20] From the hysteresis loops the coercivity ($H_c$) and the Kerr signal in remanence ($M_r$) were measured. The result is shown in Fig. 7 where the open squares are $M_r$ points (left axis) and the solid circles are values of $H_c$ (right axis) as a function of $t_{\mathrm{FeMn}}$. The lines superimposed to the experimental points are guides to the eye. The inset in the figure displays for comparison the hysteresis loops (Kerr intensity versus external applied field) for $t_{\mathrm{FeMn}} = 0$, that is, for the 6-ML Co/Cu(001) film, and for $t_{\mathrm{FeMn}} = 12$-ML $Fe_{50}Mn_{50}$ on top of 6-ML Co/Cu(001). The pronounced increase of $H_c$ starting at $t_{\mathrm{FeMn}} \approx 10$ ML ($\approx 20$ times from $t_{\mathrm{FeMn}} = 9.5$ ML to $t_{\mathrm{FeMn}} = 12$ ML) is the indication that AFM ordering in the $Fe_{50}Mn_{50}$ film is established at that thickness, i.e., $Fe_{50}Mn_{50}$ films thicker than 10 ML are AFM at room temperature. Comparable results have also been obtained upon reversing the order of deposition, when the Co film is deposited on top of the $Fe_{50}Mn_{50}$ film. Due to the interaction between the antiferromagnet and the Co film, the coercive field of the bilayer is strongly increased compared to that of the pure FM film. The increase in $H_c$ due to

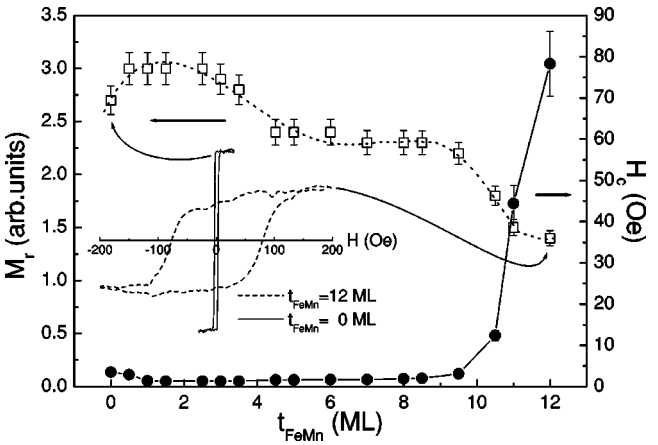


FIG. 7. Remanence $M_r$ (left axis) and coercive field $H_c$ (right axis) as a function of $Fe_{50}Mn_{50}$ film thickness ($t_{\mathrm{FeMn}}$) at 315 K. The external field was applied along the [110] azimuth direction of the Cu substrate. The values at $t_{\mathrm{FeMn}} = 0$ correspond to the remanence and coercive field of a 6-ML Co/Cu(001). The inset displays MOKE hysteresis loops for 6-ML Co/Cu(001) (solid line) and 12-ML $Fe_{50}Mn_{50}$/6-ML Co/Cu(001) (dotted line).

the AFM ordering of $Fe_{50}Mn_{50}$ has been measured at a similar thickness also for $Fe_{50}Mn_{50}/Ni_{80}Fe_{20}$ (Py) bilayers on Cu(001).[21]

The variation of $M_r$ in the displayed thickness range shows a quite complicated behavior. A very similar thickness dependence has been found for the Kerr rotation or the Kerr intensity during the deposition of metallic nonmagnetic overlayers on top of magnetic films.[22,23] In those cases an oscillatory behavior superimposed to a slow decrease as a function of the overlayer thickness was recognized. The oscillations were attributed to spin-polarized quantum well states in the metallic overlayers, which influence the magneto-optical properties of the system. Due to the similarities of the experimental observation, a similar conclusion could be attempted also for the present case of $Fe_{50}Mn_{50}$ on Co, for $t_{\mathrm{FeMn}} < 10$ ML, when $Fe_{50}Mn_{50}$ is found in a paramagnetic state. One can furthermore notice that in Fig. 7 right at the increase of $H_c$, due to the AFM order established in $Fe_{50}Mn_{50}$, a correlated decrease of $M_r$ is observed, which may be related to the antiferromagnetism in the $Fe_{50}Mn_{50}$ layer. Indeed, as we have reported in a separate publication,[24] a change in easy axis from the $\langle 110 \rangle$ to the $\langle 100 \rangle$ azimuth directions is observed in a Co film coupled to an $Fe_{50}Mn_{50}$ film thicker than 10 ML. In Fig. 7, a reduction in $M_r$ by approximately a factor $1/\sqrt{2}$ from $t_{\mathrm{FeMn}} = 9.5$ ML to $t_{\mathrm{FeMn}} = 12$ ML can be seen. This can be explained by considering that the external field, applied along one of the $\langle 110 \rangle$ directions, is not able to fully saturate the magnetic film, which now has an easy magnetization axis along one of the $\langle 100 \rangle$ directions. In this case the measured remanence is just the projection along one of the $\langle 100 \rangle$ directions on one of the $\langle 110 \rangle$ directions.

If the increase in coercive field in the Co/FeMn bilayers is due to antiferromagnetism of the FeMn film, one can measure the temperature $T_{AFM}$ at which the AFM ordering disappears. Due to finite-size scaling[26] one would expect in gen-

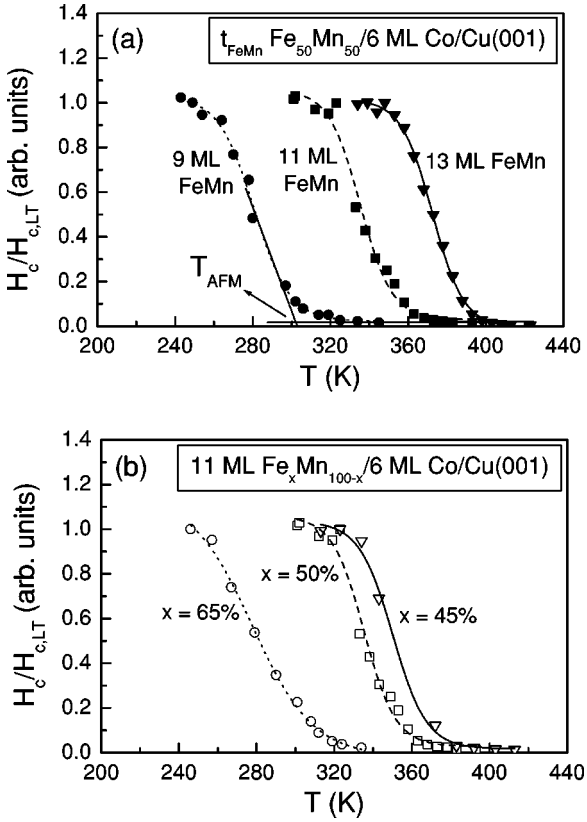


FIG. 8. (a) Normalized coercive field as a function of temperature for $t_{\mathrm{FeMn}}$ $Fe_{50}Mn_{50}$/6-ML Co/Cu(001), with $t_{\mathrm{FeMn}}=9$ ML (filled circles), 11 ML (filled squares), and 13 ML (filled triangles). For the data points of $t_{\mathrm{FeMn}}=9$ ML the way in which $T_{AFM}$ is obtained is schematically indicated. (b) Normalized coercive field as a function of temperature for 11-ML $Fe_xMn_{100-x}$/6-ML Co/Cu(001), with $x=65\%$ (open circles), $x=50\%$ (open squares), and $x=45\%$ (open triangles). The lines superimposed to the experimental points are guides to the eye.

eral a decrease of this temperature for decreasing film thickness. For thick enough films $T_{AFM}$ should approach $T_N$, the uniquely defined value of the bulk material.[25] Figure 8(a) shows the temperature dependence of the coercive field of bilayers of $Fe_{50}Mn_{50}$ layers of three different thicknesses (9, 11, and 13 ML) deposited on top of 6-ML Co/Cu(001). The values of $H_c$ have been obtained from the hysteresis loops recorded upon increasing the temperature, with the external field applied along the [110] azimuth direction of the substrate. For displaying purposes they have been normalized to the value at low temperature ($H_{c,LT}$) for each film thickness. The lines superimposed to the experimental points in Fig. 8(a) are guides to the eye. In all three curves one can see a steplike decrease of $H_c$ upon increasing the temperature. This corresponds to the crossing of $T_{AFM}$ at that thickness. The ordering temperature is shifting towards higher values for higher $t_{\mathrm{FeMn}}$. The coercive field above the ordering temperature for all the films is very similar to the coercive field of pure 6-ML Co/Cu(001) at room temperature. From these experiments one can obtain an experimental measure of $T_{AFM}$. This is done, as graphically explained for the data set of $t_{\mathrm{FeMn}}=9$ ML, by taking the intersect of the tangent of the steplike curve with the horizontal line describing the coercive field for small $t_{\mathrm{FeMn}}$. Experiments similar to the ones reported in Fig. 8(a) have been done by keeping fixed the thickness and by varying the concentration of the $Fe_xMn_{100-x}$ alloy films on top of 6-ML Co/Cu(001). In this way the concentration dependence of $T_{AFM}$ can be investigated. The result is shown in Fig. 8(b) where the normalized coercive field of 11-ML $Fe_xMn_{100-x}$/6-ML Co bilayers is plotted as a function of temperature. Open circles, open squares, and open triangles refer to Fe concentrations of $x=65\%$, $x=50\%$, and $x=45\%$, respectively. The lines superimposed to the experimental points are guides to the eye. In all three cases a marked decrease of coercive field for increasing temperature can be seen. Moreover, this decrease is present at higher temperature for lower Fe concentration in the $Fe_xMn_{100-x}$ alloy. In other words, the result of Fig. 8(b) indicates that the ordering temperature $T_{AFM}$ increases upon reducing the Fe concentration.

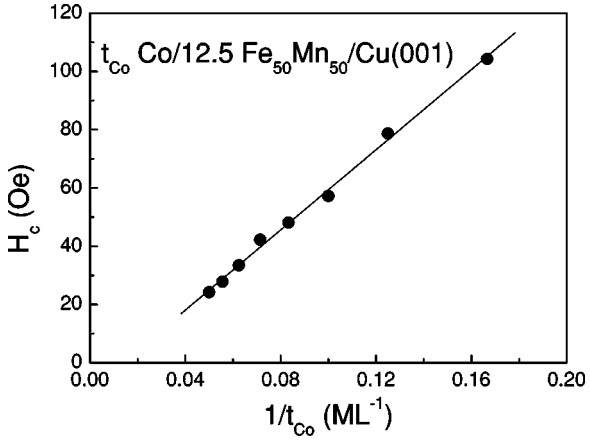


FIG. 9. Variation of coercive field as a function of the inverse of the Co thickness for $t_{\mathrm{Co}}$ Co/12.5-ML $Fe_{50}Mn_{50}$/Cu(001) films. The line superimposed to the experimental points represents the best fit with a linear function.

For $t_{\mathrm{FeMn}}>10$ ML, at 315 K, the coercivity of the Co/$Fe_{50}Mn_{50}$ is mainly caused by the magnetic interface interaction of Co with AFM $Fe_{50}Mn_{50}$. In order to investigate the ferromagnetic layer thickness dependence of the coercive field, Co films of increasing thickness were deposited on top of 12.5 ML $Fe_{50}Mn_{50}$/Cu(001). Hysteresis loops were recorded at room temperature (315 K) at each step of Co evaporation with the external field applied along the [110] azimuth direction. The measured values of $H_c$ are displayed in Fig. 9 as a function of the inverse of Co thickness ($1/t_{\mathrm{Co}}$). The $Fe_{50}Mn_{50}$ film thickness was chosen in such a way as to have the alloy in an AFM state at room temperature, as concluded from the experiments described in Fig. 7. From Fig. 9 one can see that the coercive field is monotonically decreasing upon increasing $t_{\mathrm{Co}}$. The solid line superimposed to the experimental points is the best fit with a linear function, which describes the linear dependence of the coercive field on the inverse of the Co thickness.

As outlined in the introduction one of the consequences of the FM-AFM interaction is a hysteresis loop with an enhanced coercive field. In order to obtain a hysteresis loop

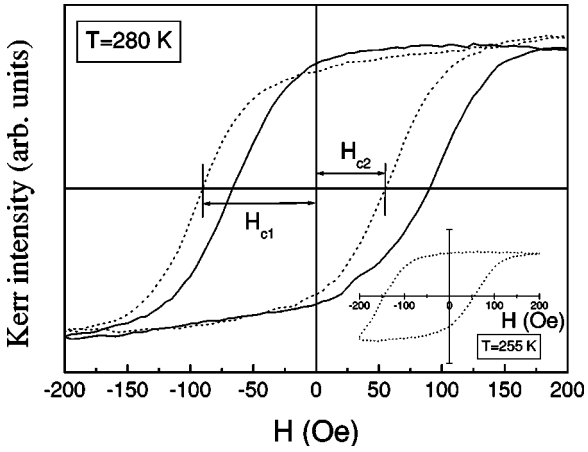


FIG. 10. Hysteresis loops from a 15-ML Co/20-ML $Fe_{50}Mn_{50}$/Cu(001) sample for two opposite field cooling directions (dotted and solid lines) measured at 280 K. In the inset a hysteresis loop from the same sample measured at 255 K is displayed.

shifted by $H_{eb}$ along the applied field axis, a pinning direction must be set. This is usually obtained by growing the AFM material under an applied field, or by cooling through the Néel temperature under an applied field. The samples studied in the present work typically displayed low values of $H_{eb}$ compared to the values of $H_c$. An example is shown in Fig. 10. Here a 15-ML Co/20-ML $Fe_{50}Mn_{50}$/Cu(001) bilayer was evaporated at room temperature and then annealed at $\approx$420 K. During cooling down to 230 K a field of 1 kOe supplied by a permanent magnet was applied along the [110] azimuth direction. The positive direction of the field of the permanent magnet coincides with the positive direction of the field applied during recording the MOKE hysteresis loops. The hysteresis loop displayed in the figure by the full line has been then recorded at 280 K, after field cooling in the negative direction. The loop is displaced from the origin of the horizontal axis towards positive values of external field as a ''normal'' exchange bias loop. By repeating the field cooling procedure with reversed field of the permanent magnet, the hysteresis loop, recorded again at 280 K, is shifted towards the negative direction. This is displayed by the dotted-line loop. In this second loop the left and right coercive fields are indicated as $H_{c1}$ and $H_{c2}$, respectively. The exchange bias and coercive fields measured from the loop are about 15 Oe and 70 Oe, respectively. By decreasing the temperature both quantities increase as one can see in the inset of Fig. 10, where a hysteresis loop measured at 255 K after field cooling in the positive direction is shown. This loop is already not completely saturated by the maximum available field of 200 Oe for negative values of applied field.

## IV. DISCUSSION

$Fe_xMn_{100-x}$ thin films have been shown in the previous section to present MEED oscillations when growing on Cu(001) and on Co/Cu(001), in a range between $x \approx 30$ at. % and $x=100$ at. % at room temperature. This is an indication that the alloy films are growing in a pseudomorphic layer-by-layer mode. This forced epitaxial growth

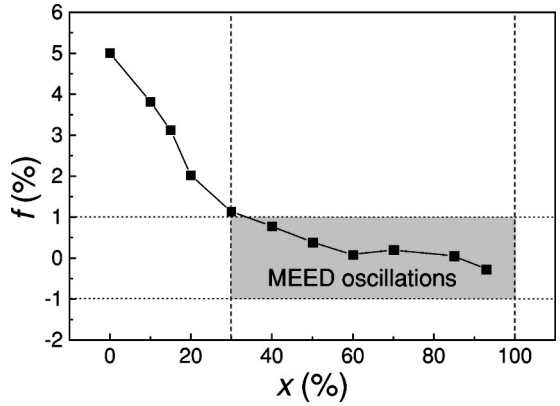


FIG. 11. Lattice misfit $f$ between the Cu and $Fe_xMn_{100-x}$ bulk alloy in the $\gamma$ phase as a function of Fe concentration $x$. $f$ has been calculated by taking the lattice parameters of $Fe_xMn_{100-x}$ as a function of $x$ from Ref. 6.

mode is favored by the small lattice misfit ($f$) between the Cu(001) substrate and the $Fe_xMn_{100-x}$ alloy. The lattice misfit is defined by the expression

$$f=\frac{a-s}{s}, \tag{2}$$

where $a$ and $s$ are the lattice parameters of the film and the substrate, respectively.

In Fig. 11 the lattice misfit between the Cu and $Fe_xMn_{100-x}$ bulk alloy is shown as a function of the Fe concentration $x$. The line connecting the points is a guide to the eye. The lattice parameter of the $Fe_xMn_{100-x}$ alloy has been taken from Ref. 6, where the $\gamma$ phase was stabilized in the full range of composition by adding a small amount of Cu (5 at. %) for $x<40$ at. % and of C (4 at. %) for $x>80$ at. %. The two vertical dashed lines in the figure delimit the concentration range in which MEED oscillations have been observed, that is, the region in which the $Fe_xMn_{100-x}$ alloy films grow in a layer-by-layer fashion on Cu(001) and on Co/Cu(001). As outlined by the gray rectangular box, the MEED oscillations are observed when the lattice misfit is approximately in the range $-1\%<f<+1\%$. One therefore can conclude that a small lattice misfit is a prerequisite for the epitaxial growth of the system under investigation.

This analysis is actually just qualitative from several points of view. At first, having a lattice misfit in the range $f=\pm 1\%$ is not a general limit for epitaxial growth. Indicative is, for example, the case of a Co thin film grown on Cu(001). This system has a lattice misfit of $f=1.8\%$, and still the layer-by-layer growth mode has been deduced from the presence of MEED oscillations.[18] Moreover, one has to consider that the fcc structure of the studied $Fe_xMn_{100-x}$ thin films has not been proven for the full range of composition, but just for the alloy at the equiatomic concentration. On the other hand an fcc structure has been reported for pure Fe grown on Cu(001) at least for a thickness range between 4 and 10 ML.[27] Intuitively one could therefore expect an fcc structure for the $Fe_xMn_{100-x}$ alloy films at least in a range of composition between $x=100$ at. % and $x=50$ at. %. When

$x$ becomes much smaller than 45 at.% (limit for the fcc structure in bulk $Fe_xMn_{100-x}$), a structural change can indeed be expected in the alloy films. For example, an hcp phase has been reported in bulk $Fe_xMn_{100-x}$ alloys at room temperature between $x=12$ and $x=30$ at.%.[28] These observations, namely, a departure from the fcc phase for low Fe content in the alloy, are consistent with the present results of the absence of MEED oscillations at room temperature for $x<30$ at.%. A change in the structure of the growing film can in fact lead to a growth mode more complicated than a simple layer-by-layer growth.

By comparing Figs. 1(a) and 1(b) one furthermore notices that the second maximum in the MEED intensity is missing for FeMn films grown on Cu(001), except for the $Fe_{95}Mn_5$ film, while it is present for FeMn films deposited on Co/Cu(001). This aspect has not been investigated in detail, and a clear explanation for this observation is not yet available. The missing MEED intensity oscillation maximum can be related to an imperfect layer-by-layer growth in the first stages of deposition of the FeMn films on Cu(001). In this respect one can make a comparison with the Fe/Cu(001) system: Fe films deposited via thermal evaporation on Cu(001) present a missing or reduced first maximum in the intensity of the diffracted electron beam, while an improved growth mode, characterized by regular intensity oscillations starting from the first atomic layer, has been obtained by pulsed laser deposition of the Fe films.[29] The imperfect initial growth of FeMn films on Cu(001) may be associated with structural rearrangements or the formation of chemically mixed interfacial layers. It remains to be explained why this would happen just in the case of growth on Cu(001) and not on Co/Cu(001), considering that from a structural point of view the situation should be rather similar. In this context one may remember that the submonolayer growth of Mn is known to lead to the formation of a two-dimensional surface alloy both in the case of Mn/Cu(001) (Ref. 30) and in the case of Mn/Co(001).[31] A possible speculation is related to the fact that in the FeMn/Co/Cu(001) system FeMn is growing on a magnetic substrate. Our recent experiments reveal that Fe and Mn in an FeMn alloy film acquire induced magnetic moments when in contact with a FM Co film.[32] If the induced moments are mainly located at the interface with Co, FeMn films are partially ferromagnetic in the first stages of growth on top of Co/Cu(001), while they are not when growing on Cu(001). The different initial growth mode of the FeMn films could be due to the different magnetic properties that the FeMn films have when growing on the two different substrates.

The fcc structure of the $Fe_{50}Mn_{50}$ alloy film deserves some further comments. Polycrystalline sputtered $Fe_{50}Mn_{50}$ films have been stabilized in the fcc structure on substrates promoting the fcc growth, as Cu (Refs. 33 and 34) or $Ni_{80}Fe_{20}$.[33,35] In the previous section the fcc structure of epitaxially grown $Fe_{50}Mn_{50}$ films has been deduced from the results of the LEED experiments. The ordered LEED pattern up to the maximum thickness investigated (26-ML $Fe_{50}Mn_{50}$) and the value of vertical interlayer distance indicate that the film is a single crystal in registry with the substrate. This is in contradiction to Ref. 21, where a polycrystalline growth of $Fe_{50}Mn_{50}$ on Cu was suggested. The stabilization of the antiferromagnetic fcc $\gamma$ phase is a particularly important point especially in view of possible applications in spin valves. The bcc $\alpha$ phase and the hcp $\epsilon$ phase, both present in the phase diagram of $Fe_xMn_{100-x}$ alloys, would lower the AFM ordering temperature of the $Fe_{50}Mn_{50}$ layer, thus reducing the thermal stability of the spin valve. It has been indeed observed that in polycrystalline $Fe_{50}Mn_{50}$/Py bilayers a highly textured fcc phase induces a higher value of both the exchange bias field and the blocking temperature.[36]

Generally the lack of a net magnetization renders the study of the magnetic properties of AFM materials difficult. On the other hand an FM material, in an exchange interacting FM-AFM bilayer, can be used as a probe of the magnetic order of the AFM material. This approach has been used in the present paper to identify the thickness-dependent transition from paramagnetic to AFM of an $Fe_{50}Mn_{50}$ thin film. The steep increase of the coercive field of a thin Co layer, when the adjacent $Fe_{50}Mn_{50}$ layer thickness overcomes $\approx 10$ ML (see Fig. 7), is due to the interaction of Co with an AFM ordered $Fe_{50}Mn_{50}$ film. Indeed a coercivity enhancement is one of the fingerprints of the FM-AFM interaction. In other words a 10-ML-thick $Fe_{50}Mn_{50}$ film would have an AFM ordering temperature around room temperature. This value is lower than the Néel temperature of bulk $Fe_{50}Mn_{50}$ ($\approx 500$ K).[6] This difference can be attributed to finite-size effects.[26] A decrease of the AFM ordering temperature by reducing the film thickness has been reported for other AFM materials such as CoO (Ref. 37) and NiO.[38] One could object that the increase in coercive field is a somewhat indirect way to measure the AFM ordering temperature, especially considering that often in thin films the coercivity is related to microstructural parameters. On the other hand the change in the Co domain configuration at the same $Fe_{50}Mn_{50}$ thickness at which the increase in $H_c$ has been measured[24] supports this interpretation. Moreover, the measured AFM ordering temperature has been shown to shift towards higher values for increasing $Fe_{50}Mn_{50}$ thickness, an observation that is consistent with a finite size effect argument.

It should be pointed out that in the above discussion we did not take into account proximity effects associated with the presence of the FM Co layer. More correctly, in fact, the measured antiferromagnetic ordering temperature should be considered representative for the $Fe_{50}Mn_{50}$ film in the $Fe_{50}Mn_{50}$/Co bilayers, rather than for the antiferromagnetic film as such. On the other hand, as pointed out in the previous section, an increase in coercivity due to the AFM ordering of $Fe_{50}Mn_{50}$ has been measured at a similar thickness as found here also for $Fe_{50}Mn_{50}/Fe_{19}Ni_{81}$ bilayers on Cu(001),[21] which suggests a similar antiferromagnetic ordering temperature for $Fe_{50}Mn_{50}$ films both coupled to Co and $Fe_{19}Ni_{81}$. However, considering the different spin structure, one can imagine that proximity effects of an FM material on an AFM material are expected to be considerably weaker than that of an FM material on an FM material.

In addition the coercive field of the $Fe_{50}Mn_{50}$/Co bilayer has been shown (see Fig. 9) to scale linearly with the inverse of the Co thickness. This behavior has been attributed to the

presence of energy losses in the AFM material in a recent model by Stiles and McMichael.[39] In this model the coercivity of an exchange biased FM-AFM bilayer can stem from two mechanisms: (i) inhomogeneous magnetization reversal, dominant at low temperature and high AFM thicknesses, which leads to a decrease of the coercive field proportional to $t_{FM}^{-2}$ (where $t_{FM}$ is the FM thickness); and (ii) irreversible magnetization changes in the AFM material, more relevant at high temperature, which cause a decrease of the coercive field like $t_{FM}^{-1}$. By increasing the $Fe_{50}Mn_{50}$ thickness on top of an FM Co thin film, the coercivity of the system increases at that thickness at which the $Fe_{50}Mn_{50}$ layer becomes AFM. In fact when the AFM order is established, the spins in the antiferromagnet will couple to the FM material and are dragged during a magnetization loop by the Co magnetization, inducing the increased coercivity. At this $Fe_{50}Mn_{50}$ thickness in fact the AFM ordering temperature is still close to room temperature, and one is in the regime where the energy losses are predominantly due to irreversible transitions in the AFM material.

By analogy with the $Fe_xMn_{100-x}$ alloy at equiatomic concentration, the increase in coercive field has been used to estimate the AFM ordering temperature also for other composition values. As a result, see Fig. 8(b), the AFM ordering temperature has been found to increase monotonically with increasing Mn content. This is not fully in agreement with the variation of the Néel temperature as a function of concentration in bulk alloys and, in particular, with the maximum for $T_N$ found at $x \approx 50$ at. %.[6] This difference could be attributed to a different magnetic behavior of the alloy in the thin-film form. On the other hand, what has been found from Fig. 8 is a transition temperature which is thickness dependent. In principle, one cannot exclude that films with different concentrations present different finite-size effects. Additionally one has to consider that in Ref. 6 the fcc structure for the high Mn concentration range was stabilized by adding a small amount of Cu. In Ref. 40 a linear decrease of the Néel temperature of bulk $Fe_xMn_{100-x}$ has been observed by adding a small amount of Cu and the extrapolated value of $T_N$ at zero Cu contents increases almost monotonically by increasing the Mn content. In particular the maximum at $x = 50$ at. % was not observed. This would be more in line with the present results on thin films.

## V. CONCLUSION

The structural and magnetic properties of thin FeMn films have been studied in this work. Special attention has been brought to the alloy at equiatomic concentration, relevant for applications in spin valve structures. A layer-by-layer growth mode of $Fe_{50}Mn_{50}$ on Cu(001) and on Co/Cu(001) has been deduced from the presence of oscillations in the medium-energy electron-diffraction intensity recorded during deposition. The AFM fcc $\gamma$ phase of the bulk $Fe_{50}Mn_{50}$ alloy is conserved also in thin films, as demonstrated by the low-energy electron-diffraction patterns obtained after deposition of the alloy on Cu(001) and on Co/Cu(001).

The magnetic behavior has been studied by recording magnetization curves, exploiting the magneto-optic Kerr effect. The coercive field of the $Co/Fe_{50}Mn_{50}$ bilayers displays, at room temperature, a large increase of more than one order of magnitude, when the $Fe_{50}Mn_{50}$ thickness overcomes approximately 10 ML. This increase in coercivity is attributed to the coupling of the FM Co film to the AFM $Fe_{50}Mn_{50}$ film. A 10-ML-thick $Fe_{50}Mn_{50}$ film has therefore an AFM ordering temperature around room temperature. This value is lower than the Néel temperature of the bulk material ($\approx 500$ K). The temperature and $Fe_{50}Mn_{50}$ thickness dependence of the increase in coercive field suggest that this is due to the reduced dimensionality of the film with respect to the bulk. $T_{AFM}$ also depends on the concentration of the $Fe_xMn_{100-x}$ alloy films, monotonically increasing with the increase of the Mn concentration.

## ACKNOWLEDGMENTS

We would like to thank B. Zada for her expert technical support and express our gratitude to T. Igel, R. Pfandzelter, and H. Winter for the supply of the first Mn pieces. Thanks are due to J. Barthel and L. Chelaru for a critical reading of the manuscript. Financial support by the German Minister for Education and Research (BMBF) under Grant No. 05 KS1EFA 6 and hospitality by the Berliner Elektronenspeicherring-Gesellschaft für Synchrotronstrahlung (BESSY) are gratefully acknowledged.

[1] B. Dieny, V. S. Speriosu, S. S. P. Parkin, B. A. Gurney, D. R. Wilhoit, and D. Mauri, Phys. Rev. B **43**, 1297 (1991).
[2] W. H. Meiklejohn and C. P. Bean, Phys. Rev. **102**, 1413 (1956).
[3] J. Nogués and I. K. Schuller, J. Magn. Magn. Mater. **192**, 203 (1999).
[4] M. Kiwi, J. Magn. Magn. Mater. **234**, 584 (2001).
[5] H. Umebayashi and Y. Ishikawa, J. Phys. Soc. Jpn. **21**, 1281 (1966).
[6] Y. Endoh and Y. Ishikawa, J. Phys. Soc. Jpn. **30**, 1614 (1971).
[7] J. C. S. Kools, IEEE Trans. Magn. **32**, 3165 (1996).
[8] K.-M. H. Lenssen, A. E. M. De Veirman, and J. J. T. M. Donkers, J. Appl. Phys. **81**, 4915 (1997).
[9] L. Tang, D. E. Laughlin, and S. Gangopadhyay, J. Appl. Phys. **81**, 4906 (1997).
[10] H. N. Fuke, K. Saito, Y. Kamiguchi, H. Iwasaki, and M. Sahashi, J. Appl. Phys. **81**, 4004 (1997).
[11] K. M. Krishnan, C. Nelson, C. J. Echer, R. F. C. Farrow, R. F. Marks, and A. J. Kellock, J. Appl. Phys. **83**, 6810 (1998).
[12] *Handbook of Chemistry and Physics*, edited by D. R. Lide (CRC Press, Boca Raton, 2001).
[13] J. B. Pendry, *Low Energy Electron Diffraction* (Academic Press, New York, 1974).
[14] F. Baudelet, M.-T. Lin, W. Kuch, K. Meinel, B. Choi, C. M. Schneider, and J. Kirschner, Phys. Rev. B **51**, 12 563 (1995).

[15] J. Thomassen, F. May, B. Feldmann, M. Wuttig, and H. Ibach, Phys. Rev. Lett. **69**, 3831 (1992).
[16] J. H. Neave, B. A. Joyce, P. J. Dobson, and N. Norton, Appl. Phys. A: Solids Surf. **31**, 1 (1983).
[17] S. T. Purcell, B. Heinrich, and A. S. Arrott, Phys. Rev. B **35**, 6458 (1987).
[18] C. M. Schneider, A. K. Schmid, P. Schuster, H. P. Oepen, and J. Kirschner, in *Magnetism and Structure in Systems of Reduced Dimension*, edited by R. F. C. Farrow, B. Dieny, M. Donath, A. Fert, and B. D. Hermsmeier (Plenum Press, New York, 1993).
[19] C. M. Schneider, P. Bressler, P. Schuster, J. Kirschner, J. J. de Miguel, R. Miranda, and S. Ferrer, Vacuum **41**, 503 (1990).
[20] P. Krams, F. Lauks, R. L. Stamps, B. Hillebrands, and G. Güntherodt, Phys. Rev. Lett. **69**, 3674 (1992).
[21] R. Jungblut, R. Coehoorn, M. T. Johnson, J. aan de Stegge, and A. Reinders, J. Appl. Phys. **75**, 6659 (1994).
[22] R. Mégy, A. Bounouh, Y. Suzuki, P. Beauvillain, P. Bruno, C. Chappert, B. Lecuyer, and P. Veillet, Phys. Rev. B **51**, 5586 (1995).
[23] W. Weber, A. Bischof, R. Allenspach, C. Würsch, C. H. Back, and D. Pescia, Phys. Rev. Lett. **76**, 3424 (1996).
[24] W. Kuch, F. Offi, L. I. Chelaru, M. Kotsugi, K. Fukumoto, and J. Kirschner, Phys. Rev. B **65**, 140408(R) (2002).
[25] In binary alloys actually the Néel temperature is not a uniquely defined quantity also in the bulk, since it depends on the chemical order and the composition of the system. For simplicity throughout the paper we used the definitions of Néel temperature ($T_N$) as the temperature at which antiferromagnetic order disappears in bulk FeMn, and antiferromagnetic ordering temperature ($T_{AFM}$) as the temperature at which antiferromagnetic order disappears in thin FeMn films coupled to Co films. While $T_N$ depends just on the composition of FeMn, $T_{AFM}$ depends on both the thickness and the composition of the FeMn films.
[26] See, for example, P. Poulopoulos and K. Baberschke, J. Phys.: Condens. Matter **11**, 9495 (1999).
[27] See for example, P. Bayer, S. Müller, P. Schmailzl, and K. Heinz, Phys. Rev. B **48**, 17 611 (1993).
[28] *Binary Alloy Phase Diagrams*, edited by T. B. Massalski and H. Okamoto (American Society for Metals, Metals Park, OH, 1990).
[29] H. Jenniches, J. Shen, C. V. Mohan, S. S. Manoharan, J. Barthel, P. Ohresser, M. Klaua, and J. Kirschner, Phys. Rev. B **59**, 1196 (1999).
[30] M. Wuttig, Y. Gauthier, and S. Blügel, Phys. Rev. Lett. **70**, 3619 (1993).
[31] B.-C. Choi, P. J. Bode, and J. A. C. Bland, Phys. Rev. B **58**, 5166 (1998).
[32] F. Offi, W. Kuch, L. I. Chelaru, K. Fukumoto, M. Kotsugi, and J. Kirschner (unpublished).
[33] C. Tsang, N. Heiman, and K. Lee, J. Appl. Phys. **52**, 2471 (1981).
[34] R. D. Hemstead, S. Krongelb, and D. A. Thompson, IEEE Trans. Magn. **14**, 521 (1978).
[35] C. Hwang, R. H. Geiss, and J. K. Howard, J. Appl. Phys. **64**, 6115 (1988).
[36] G. Choe and S. Gupta, Appl. Phys. Lett. **70**, 1766 (1997).
[37] T. Ambrose and C. L. Chien, Phys. Rev. Lett. **76**, 1743 (1996).
[38] D. Alders, L. H. Tjeng, F. C. Voogt, T. Hibma, G. A. Sawatzky, C. T. Chen, J. Vogel, M. Sacchi, and S. Iacobucci, Phys. Rev. B **57**, 11 623 (1998).
[39] M. D. Stiles and R. D. McMichael, Phys. Rev. B **63**, 064405 (2001).
[40] O. A. Khomenko, I. F. Khil'kevich, G. Y. Zvigintseva, L. A. Vaganova, and M. M. Belenkova, Phys. Met. Metallogr. **47**, 180 (1980).